Appl Phys A (2013) 113:483–490
DOI 10.1007/s00339-013-7551-4

Applied Physics A
Materials Science & Processing

Mechanical properties of *g*-GaN: a first principles study

Qing Peng · Chao Liang · Wei Ji · Suvranu De

Received: 4 September 2012 / Accepted: 7 January 2013 / Published online: 24 January 2013
© Springer-Verlag Berlin Heidelberg 2013

Abstract We investigate the mechanical properties of proposed graphene-like hexagonal gallium nitride monolayer (*g*-GaN) using first-principles calculations based on density-functional theory. Compared to the graphene-like hexagonal boron nitride monolayer (*g*-BN), *g*-GaN is softer, with 40 % in-plane stiffness, 50 %, 46 %, and 42 % ultimate strengths in *armchair*, *zigzag*, and *biaxial* strains, respectively. However, *g*-GaN has a larger Poisson's ratio, 0.43, about 1.9 times that of *g*-BN. It was found that the *g*-GaN also sustains much smaller strains before rupture. We obtained the second-, third-, fourth-, and fifth-order elastic constants for a rigorous continuum description of the elastic response of *g*-GaN. The second-order elastic constants, including in-plane stiffness, are predicted to monotonically increase with pressure while the Poisson's ratio monotonically decreases with increasing pressure. The sound velocity of a compressional wave has a minima of 10 km/s at an in-plane pressure of 1 N/m, while as a shear wave's velocity monotonically increases with pressure. The tunable sound velocities have promising applications in nano waveguides and surface acoustic wave sensors.

1 Introduction

The hexagonal gallium nitride monolayer (*g*-GaN) is a proposed graphene-like 2D material (Fig. 1), and it has attracted considerable interest due to its promising applications in optoelectronics and energy engineering [1]. Different from *h*-GaN, which is bulk hexagonal gallium nitride with wurtzite structure (space group $P63mc$), *g*-GaN is only monatomically thick. In contrast to GaN nanowires [2, 3] and nanoribbons [4], *g*-GaN has not been fabricated yet. However, the theoretical study of *g*-GaN can expand the range of possible applications of well-known graphene and its BN analogues, *g*-BN [5], and open new perspectives for miniaturization in engineering functional nanodevices and interconnects by a chemical modification. A previous first-principles study shows that *g*-GaN has a bond length of 1.85 Å, cohesive energy of 12.74 eV, in-plane stiffness of 110 J/m^2, Poisson ratio of 0.48, and an indirect band gap of 5 eV [6]. With a predicted wide band gap, *g*-GaN is a good candidate for fabrication of energy-efficient, reliable long-lifetime deep-UV light emitting diodes, intended for applications in sustainable water/air purification and biomedical systems, as well as photovoltaic applications [7, 8]. It is also applicable for design and preparation of multilayer antireflection and protection coatings of infrared (IR) windows.

Mechanical properties are critical in designing parts or structures with *g*-GaN for practical applications. Strain engineering is a common and important approach to tailor the functional and structural properties of nanomaterials [9]. One can expect that the properties of *g*-GaN will be affected by applied strain, also. In addition, *g*-GaN is vulnerable to strain with or without intent because of the monatomic thickness. For example, there are strains because of the mismatch of lattice constants or surface corrugation with substrates [10, 11]. Therefore, the knowledge of mechanical properties of *g*-GaN is highly desired.

Depending on the loading, the mechanical properties are divided into four strain domains: linear elastic, nonlinear elastic, plastic, and fracture. Materials in the first two strain domains are reversible, i.e., they can return to equilibrium status after the release of the loads. On the contrary, the last

Q. Peng (✉) · C. Liang · W. Ji · S. De
Department of Mechanical, Aerospace and Nuclear Engineering, Rensselaer Polytechnic Institute, Troy, NY 12180, USA
e-mail: qpeng.org@gmail.com

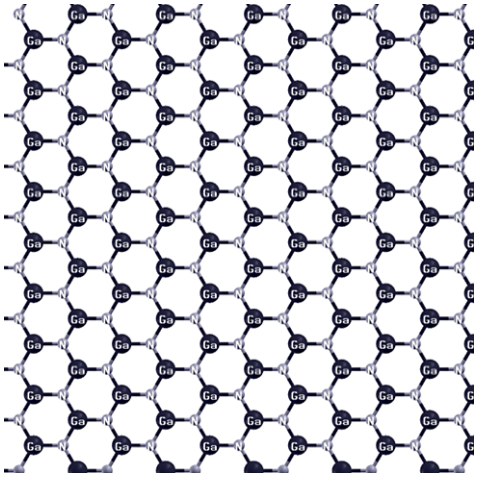

Fig. 1 g-GaN: graphene-like hexagonal gallium nitride monolayer

two domains are non-reversible. Defects are nucleated and accumulated with the increase in strain until rupture. As in graphene, the nonlinear mechanical properties are prominent since it remains elastic until the intrinsic strength is reached [12, 13]. Thus, it is of great interest to examine the nonlinear elastic properties of g-GaN, which is necessary to understand the strength and reliability of structures and devices made of g-GaN.

Several previous studies have shown that 2D monolayers present a large nonlinear elastic deformation during the tensile strain up to the ultimate strength of the material, followed by a strain softening until fracture [13–15]. We expect that the g-GaN behaves in a similar manner. Under large deformation, the strain energy density needs to be expanded as a function of strain in a Taylor series to include quadratic and higher order terms. The higher order terms account for both nonlinearity and strain softening of the elastic deformation. They can also express other anharmonic properties of 2D nanostructures including phenomena such as thermal expansion, phonon–phonon interaction, etc. [12].

The goal of this paper is to study the mechanical behaviors of g-GaN at large strains and find an accurate continuum description of the elastic properties from ab initio density functional theory calculations. The total energies of the system, forces on each atoms, and stresses on the simulation boxes are directly obtained from DFT calculations. The response of g-GaN under the nonlinear deformation and fracture is studied, including ultimate strength and ultimate strain. The high order elastic constants are obtained by fitting the stress–strain curves to analytical stress–strain relationships that belong to the continuum formulation [14]. We compared this proposed new material with the well-known 2D materials such as g-BN, and graphene. Based on our result of the high order elastic constants, the pressure dependence properties, such as sound velocities and the second-order elastic constants, including the in-plane stiffness, are

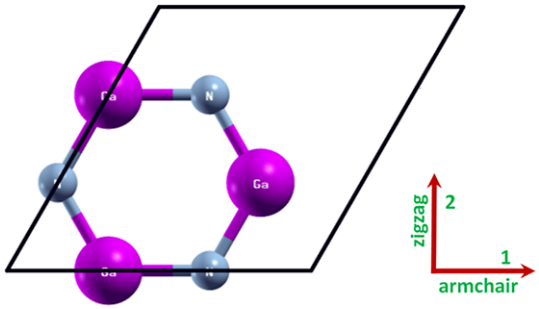

Fig. 2 Atomic structure of g-GaN in the conventional unit cell (6 atoms) in the undeformed reference configuration

predicted. Our results for the continuum formulation could also be useful in finite element modeling of the multiscale calculations for mechanical properties of g-GaN at the continuum level. The remainder of the paper is organized as follows. Section 2 presents the computational details of the DFT calculations. The results and analysis are in Sect. 3, followed by conclusions in Sect. 4.

2 Density functional theory calculations

We consider a conventional unit cell containing 6 atoms (3 gallium atoms and 3 nitrogen atoms) with periodic boundary conditions (Fig. 2). The 6-atom conventional unit cell is chosen to capture the "soft mode," which is a particular normal mode exhibiting an anomalous reduction in its characteristic frequency and leading to mechanical instability. This soft mode is a key factor in limiting the strength of monolayer materials that can only be captured in unit cells with hexagonal rings [16].

The total energies of the system, forces on each atoms, stresses, and stress–strain relationships of g-GaN under the desired deformation configurations are characterized via first-principles calculations with density-functional theory (DFT). DFT calculations were carried out with the Vienna Ab-initio Simulation Package (VASP) [17–20] which is based on the Kohn–Sham Density Functional Theory (KS-DFT) [21, 22] with the generalized gradient approximations as parameterized by Perdew, Burke, and Ernzerhof (PBE) for exchange-correlation functions [23]. The electrons explicitly included in the calculations are the $(2s^2 2p^2)$ electrons for nitrogen atoms and $(3d^{10} 4s^2 4p^1)$ electrons for gallium atoms. The core electrons are replaced by the projector augmented wave (PAW) and pseudo-potential approach [24, 25]. A plane-wave cutoff of 600 eV is used in all the calculations. The calculations are performed at zero temperature.

The criterion to stop the relaxation of the electronic degrees of freedom is set by the total energy change to be smaller than 0.000001 eV. The optimized atomic geometry was achieved through minimizing Hellmann–Feynman

forces acting on each atom until the maximum forces on the ions were smaller than 0.001 eV/Å.

The atomic structures of all the deformed and undeformed configurations were obtained by fully relaxing a 6-atom-unit cell where all atoms were placed in one plane. The simulation invokes periodic boundary conditions for the two in-plane directions while the displacement to out-of-plane direction is forbidden.

The irreducible Brillouin zone was sampled with a Gamma-centered $17 \times 17 \times 1$ k-mesh. Such a large k-mesh was used to reduce the numerical errors caused by the strain of the systems. The initial charge densities were taken as a superposition of atomic charge densities. There was a 15 Å vacuum region to reduce the interlayer interaction to model the single layer system. To eliminate the artificial effect of the out-of-plane thickness of the simulation box on the stress, we used the second Piola–Kirchhoff stress [14] to express the 2D forces per length with units of N/m.

For a general deformation state, the number of independent components of the second-, third-, fourth-, and fifth-order elastic tensors are 21, 56, 126, and 252, respectively. However, there are only fourteen independent elastic constants that need to be explicitly considered due to the symmetries of the atomic lattice point group D_{6h}, which consists of a six-fold rotational axis and six mirror planes [13].

The fourteen independent elastic constants of g-GaN are determined by a least-squares fit to the stress–strain results from DFT based first-principles studies in two steps, detailed in our previous work in g-BN [14], which had also been well used to explore the mechanical properties of grahyne [15], graphane [26], g-TlN [27], and g-ZnO [28]. A brief introduction is that, in the first step, we use a least-squares fit of five stress–strain responses. Five relationships between stress and strain are necessary because there are five independent fifth-order elastic constants (FFOEC). We obtain the stress–strain relationships by simulating the following deformation states: uniaxial strain in the zigzag direction (*zigzag*), uniaxial strain in the armchair direction (*armchair*), and equibiaxial strain (*biaxial*). For each deformation direction, there are two components of the stresses. As a result, there are five independent stress–strain relationships since the two components of stress in the biaxial strain are identical. From the first step, the components of the second-order elastic constants (SOEC), the third-order elastic constants (TOEC), and the fourth-order elastic constants (FOEC) are over-determined (i.e., the number of linearly independent variables is greater than the number of constraints), and the fifth-order elastic constants are well determined (the number of linearly independent variables are equal to the number of constraints). Under such circumstances, a second step is needed: least-square solution to these over- and well-determined linear equations.

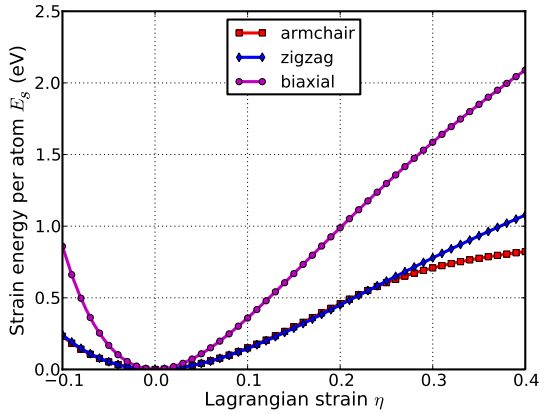

Fig. 3 Energy-strain responses for uniaxial strain in armchair and zigzag directions, and equibiaxial strains

3 Results and analysis

3.1 Atomic structure

We first optimize the equilibrium lattice constant for g-GaN. The total energy as a function of lattice spacing is obtained by specifying nine lattice constants varying from 2.8 Å to 3.6 Å, with full relaxations of all the atoms. A least-square fit of the energies versus lattice constants with a fourth-order polynomial function yields the equilibrium lattice constant as $a = 3.207$ Å. The most energetically favorable structure is set as the strain-free structure in this study and the atomic structure as well as the conventional cell is shown in Fig. 2. Specifically, the bond length of Ga-N is 1.852 Å, which is 0.402 Å (or 28 %) longer than the bond length of the B-N bond in g-BN. The N-Ga-N and Ga-N-Ga angles are 120° and all atoms are within one plane. Our result for the bond length is in good agreement with a previous first-principles study [6].

3.2 Strain energy

When the strains are applied, all the atoms are allowed full freedom of motion within their plane. A quasi-Newton algorithm is used to relax all atoms into equilibrium positions within the deformed unit cell that yields the minimum total energy for the imposed strain state of the super cell.

Both compression and tension are considered with Lagrangian strains ranging from -0.1 to 0.4 with an increment of 0.01 in each step for all three deformation modes. We define strain energy per atom $E_s = (E_{\text{tot}} - E_0)/n$, where E_{tot} is the total energy of the strained system, E_0 is the total energy of the strain-free system, and $n = 6$ is the number of atoms in the unit cell. This size-independent quantity is used for the comparison between different systems. Figure 3 shows the E_s of g-GaN as a function of strain in uniaxial armchair, uniaxial zigzag, and equibiaxial deformation.

E_s is seen to be anisotropic with strain direction. E_s is nonsymmetrical for compression ($\eta < 0$) and tension ($\eta > 0$) for all three modes. This nonsymmetry indicates the anharmonicity of the g-GaN structures. The harmonic region where the E_s is a quadratic function of applied strain can be taken between $-0.02 < \eta < 0.02$. The stresses, derivatives of the strain energies, are linearly increasing with the increase of the applied strains in the harmonic region. The anharmonic region is the range of strain where the linear stress–strain relationship is invalid and higher order terms are not negligible. With even larger loading of strains, the systems will undergo irreversible structural changes, and the systems are in a plastic region where they may fail. The maximum strain in the anharmonic region is the *critical* strain. The critical strains are not spotted in this study. The ultimate strains are determined as the corresponding strain of the ultimate stress, which is the maxima of the stress–strain curve, as discussed in the following section.

3.3 Stress–strain curves

The second P-K stress versus Lagrangian strain relationship for uniaxial strains along the armchair and zigzag directions, as well as biaxial strains are shown in Fig. 4. The stresses are the derivatives of the strain energies with respect to the strains. The ultimate strength is the maximum stress that a material can withstand while being stretched, and the corresponding strain is the ultimate strain. Under ideal conditions, the critical strain is larger than the ultimate strain. The systems of perfect g-GaN under strains beyond the ultimate strains are in a metastable state, which can be easily destroyed by long wavelength perturbations and vacancy defects, as well as high temperature effects [29]. The ultimate strain is determined by the intrinsic bonding strengths and acts as a lower limit of the critical strain. Thus, it has a practical meaning in consideration for its applications.

The ultimate strengths and strains corresponding to the different strain conditions are in Table 1, compared with that of g-BN and graphene. The material behaves in an asymmetric manner with respect to compressive and tensile strains. With increasing strains, the Ga-N bonds are stretched and eventually rupture. When the strain is applied in the armchair direction, the bonds who are parallel to this direction are more severely stretched than those in other directions. The ultimate strain in armchair deformation is 0.18 (Fig. 4 top panel), smaller than that of g-BN and graphene. Under the zigzag deformation, in which the strain is applied perpendicular to the armchair, there is no bond parallel to this direction. The bonds at an incline to the zigzag direction with an angle of 30° are more severely stretched than those in the armchair direction. The ultimate strain in this zigzag deformation is 0.22, smaller than that of g-BN and graphene. At this ultimate strain, the bonds that are at an incline to the armchair direction appear to be ruptured (Fig. 4 middle panel). Under the biaxial deformation, the ultimate strain is $\eta_m^b = 0.16$, which is the smallest among those of the three compared. As the ultimate strain is applied, all the Ga-N bonds are observed to be ruptured (Fig. 4 bottom).

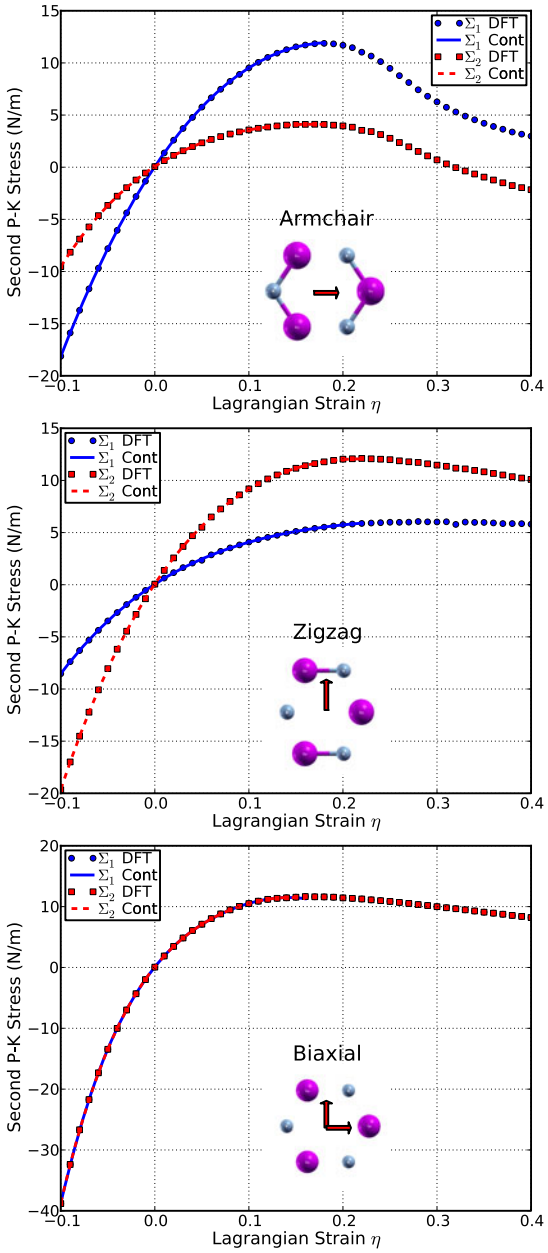

Fig. 4 Stress–strain responses of g-GaN under the armchair, zigzag, and biaxial strain. Σ_1 (Σ_2) denotes the x (y) component of stress. "Cont" stands for the fitting of DFT calculations ("DFT") to continuum elastic theory

It should be noted that the softening of the perfect g-GaN under strains beyond the ultimate strains only occur for ideal conditions. The systems under this circumstance are in a metastable state, which can be easily destroyed by long wavelength perturbations and vacancy defects, as well as high temperature effects, and enter a plastic state [29].

Table 1 Ultimate strengths (Σ_m^a, Σ_m^z, Σ_m^b) in units of N/m and ultimate strains (η_m^a, η_m^z, η_m^b) under uniaxial strain (armchair and zigzag) and biaxial from DFT calculations, compared with g-BN and graphene

	g-GaN	g-BN [14]	Graphene [26]
Σ_m^a	11.9	23.6	28.6
η_m^a	0.18	0.18	0.19
Σ_m^z	12.1	26.3	30.4
η_m^z	0.22	0.26	0.23
Σ_m^b	11.7	27.8	32.1
η_m^b	0.16	0.24	0.23

Thus, only the data within the ultimate strain have physical meaning and were used in determining the high order elastic constants in the following subsection.

3.4 Elastic constants

The elastic constants are critical parameters in finite element analysis models for mechanical properties of materials. Our results of these elastic constants provide an accurate continuum description of the elastic properties of g-GaN from ab initio density functional theory calculations. They are suitable for incorporation into numerical methods such as the finite element technique.

The second-order elastic constants model the linear elastic response. The higher (> 2) order elastic constants are important to characterize the nonlinear elastic response of g-GaN using a continuum description. These can be obtained using a least squares fit of the DFT data and are reported in Table 2. Corresponding values for graphene are also shown.

The in-plane Young's modulus Y_s and Poisson's ratio ν may be obtained from the following relationships: $Y_s = (C_{11}^2 - C_{12}^2)/C_{11}$ and $\nu = C_{12}/C_{11}$. We have $Y_s = 109.4$ (N/m) and $\nu = 0.431$, in good agreement with a previous study, which has $Y_s = 110$ (N/m) and $\nu = 0.48$ [6]. The in-plane stiffness of g-GaN is very small compared to g-BN (39 %) and graphene (32 %). The reduction of in-plane stiffness from g-BN to g-GaN is a result of the weakened bond of Ga-N compared to the B-N bond in g-BN. With all other things being equal, bond length is inversely related to bond strength and the bond dissociation energy, as a stronger bond will be shorter. Considering the bond length, in g-GaN the bond length of Ga-N is 1.852 Å, about 28 % larger than the B-N bond length in g-BN (1.45 Å). The bonds can be viewed as being prior stretched by the replacement of boron atoms with gallium atoms, in reference to g-BN. These stretched bonds are weaker than those unstretched, resulting a reduction of the mechanical strength.

Knowledge of higher order elastic constants is very useful in understanding the anharmonicity. Using the higher order elastic continuum description, one can calculate the stress and deformation state under uniaxial stress, rather than uniaxial strain [13]. Explicitly, when pressure is applied, the pressure dependent second-order elastic moduli can be obtained from the high order elastic continuum description [15, 30–32]. The third-order elastic constants are important in understanding the nonlinear elasticity of materials such as changes in acoustic velocities due to finite strain. As a consequence, nanodevices such as nanosurface acoustic wave sensors and nano waveguides could be synthesized by introducing local strain [15, 33].

Table 2 Nonzero independent components for the SOEC, TOEC, FOEC, and FFOEC tensor components, Poisson's ratio ν and in-plane stiffness Y_s of g-GaN from DFT calculations, compared with g-BN and graphene

	g-GaN	g-BN [14]	Graphene [26]
a	3.207	2.512	2.468
Y_s	109.4	278.3	340.8
ν	0.431	0.225	0.178
C_{11}	134.4	293.2	352.0
C_{12}	57.9	66.1	62.6
C_{111}	−1038.6	−2513.6	−3089.7
C_{112}	−452.2	−425.0	−453.8
C_{222}	−880.6	−2284.2	−2928.1
C_{1111}	5478	16547	21927
C_{1112}	2710	2609	2731
C_{1122}	4964	2215	3888
C_{2222}	2165	12288	18779
C_{11111}	−22786	−65265	−118791
C_{11112}	12073	−8454	−19173
C_{11122}	−29688	−28556	−15863
C_{12222}	26909	−36955	−27463
C_{22222}	−9539	−100469	−134752

It is worthy to note that the uncertainty of the high order elastic constants arises from the propagation of the numerical error of the total energy calculations. The constringency of the total energy is 10^{-6} eV. The uncertainty of the second-, third-, fourth-, and fifth-order elastic constants are 10^{-2}, 10^{0}, 10^{2}, and 10^{4}, respectively.

Stress–strain curves in the previous section show that they will soften when the strain is larger than the ultimate strain. From the view of electron bonding, this is due to the bond weakening and breaking. This softening behavior is determined by the TOECs and FFOECs in the continuum aspect. The negative values of TOECs and FFOECs ensure the softening of the g-GaN monolayer under large strain.

The hydrostatic terms (C_{11}, C_{22}, C_{111}, C_{222}, and so on) of g-GaN monolayers are smaller than those of g-BN and graphene, consistent with the conclusion that the g-GaN is "softer." The shear terms (C_{12}, C_{112}, C_{1122}, etc.) in general are smaller than those of g-BN and graphene, which contributes to the high compressibility of g-GaN. Compared to

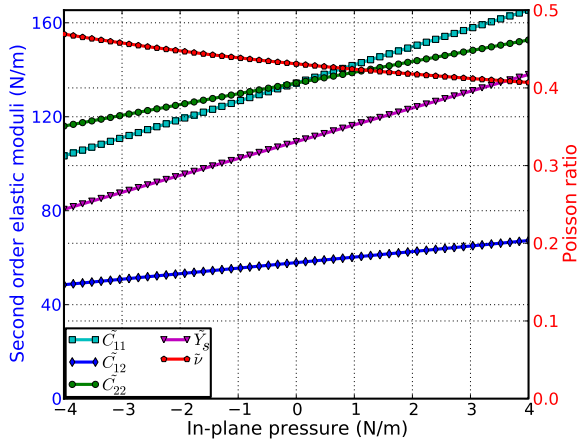

Fig. 5 Second-order elastic moduli and Poisson ratio as a function of the pressure

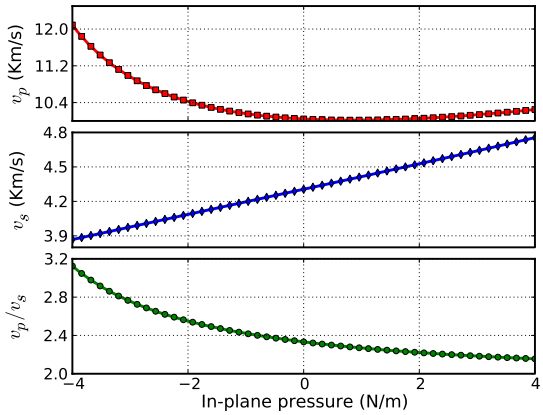

Fig. 6 p-wave and s-wave velocities, and compressional to shear wave velocity ratio v_p/v_s as a function of in-plane pressure

graphene and g-BN, one can conclude that the mechanical behavior of g-GaN is much softer than graphene and g-BN.

3.5 Effect of pressure on the elastic moduli

With third-order elastic moduli, we can study the effect of pressure on the second-order elastic moduli, where the pressure p acts in the plane of g-GaN. Explicitly, when pressure is applied, the pressure dependent second-order elastic moduli ($\tilde{C}_{11}$, $\tilde{C}_{12}$, $\tilde{C}_{22}$) can be obtained from C_{11}, C_{12}, C_{22}, C_{111}, C_{112}, C_{222}, Y_s, and ν as:

$$\tilde{C}_{11} = C_{11} - (C_{111} + C_{112})\frac{1-\nu}{Y_s}P, \tag{1}$$

$$\tilde{C}_{22} = C_{11} - C_{222}\frac{1-\nu}{Y_s}P, \tag{2}$$

$$\tilde{C}_{12} = C_{12} - C_{112}\frac{1-\nu}{Y_s}P. \tag{3}$$

The second-order elastic moduli of g-GaN are seen to increase linearly with the applied pressure (Fig. 5). However, Poisson's ratio decreases monotonically with the increase of pressure. $\tilde{C}_{11}$ is asymmetrical to $\tilde{C}_{22}$ unlike the zero pressure case. $\tilde{C}_{11} = \tilde{C}_{22} = C_{11}$ only occurs when the pressure is zero. This anisotropy could be the outcome of anharmonicity.

3.6 Promising applications

In the g-GaN monolayer, there are nonzero in-plane Young's moduli and shear deformations. Hence, it is possible to generate sound waves with different velocities depending on the deformation mode. Sound waves generating biaxial deformations (compressions) are compressional or p-waves. Sound waves generating shear deformations are shear or s-waves. The sound velocities of these two types of waves are calculated from the second-order elastic moduli and mass density using the following relations:

$$v_p = \sqrt{\frac{\tilde{Y}_s(1-\tilde{\nu})}{\rho_m(1+\tilde{\nu})(1-2\tilde{\nu})}}, \tag{4}$$

$$v_s = \sqrt{\frac{\tilde{C}_{12}}{\rho_m}}. \tag{5}$$

The dependence of v_p and v_s on pressure (biaxial stress) is plotted in Fig. 6. The minima (10 km/s) of the v_p curve occurs at an in-plane pressure of 1 N/m. However, v_s monotonically increases with an increasing pressure. Thus, they can be tuned by introducing the biaxial strain through the stress–strain relationship shown in Fig. 4c.

The compressional to shear wave velocity ratio (v_p/v_s) is a very useful parameter in the determination of a material's mechanical properties. It depends only on the Poisson's ratio as

$$\frac{v_p}{v_s} = \sqrt{\frac{1}{\tilde{\nu}}\left(1 + \frac{\tilde{\nu}^2}{1-2\tilde{\nu}}\right)}. \tag{6}$$

The ratio of v_p/v_s monotonically decreases with an increase of pressure as shown in Fig. 6. It tends to approach a value of 2.0 at positive pressure.

Notice that a sound velocity gradient could be achieved by introducing stress into g-GaN, which could lead to refraction of sound wavefronts in the direction of lower sound speed, causing the sound vectors to follow a curved path [34]. The radius of curvature of the sound path is inversely proportional to the gradient. Also, a negative sound speed gradient could be achieved by a negative strain gradient. This tunable sound velocity gradient can be used to form a sound frequency and ranging channel, which is the functional mechanism of waveguides and surface acoustic wave (SAW) sensors [35, 36]. Thus, g-GaN-based nanodevices of SAW sensors, filters, and waveguides may be synthesized using local strains for next generation electronics.

4 Conclusions

In summary, we studied the mechanical response of g-GaN under various strains using DFT based first-principles calculations. It was observed that g-GaN exhibits a nonlinear elastic deformation up to an ultimate strain, which is 0.18, 0.22, and 0.16 for armchair, zigzag, and biaxial directions, respectively. The deformation and failure behavior and the ultimate strength are anisotropic. It has a low in-plane stiffness (109.4 N/m) and a large Poisson ratio compared to g-BN and graphene. Compared to g-BN, g-GaN has 39 % in-plane stiffness, 50 %, 46 %, and 42 % ultimate strengths in *armchair*, *zigzag*, and *biaxial* strains, respectively, and the Poisson's ratio is 1.9 times larger. We also found that the g-GaN can sustain much smaller strains before rupture.

The nonlinear elasticity of g-GaN was investigated. We found an accurate continuum description of the elastic properties of g-GaN by explicitly determining the fourteen independent components of high order (up to fifth-order) elastic constants from the fitting of the stress–strain curves obtained from DFT calculations. This data is useful to develop a continuum description which is suitable for incorporation into a finite element analysis model for its applications at large scale. The second-order elastic constants including in-plane stiffness are predicted to monotonically increase with pressure while Poisson's ratio monotonically decreases with increasing pressure. The sound velocity of a compressional wave has a minima of 10 km/s at an in-plane pressure of 1 N/m, while as a shear wave's velocity monotonically increases with pressure. The ratio of v_p/v_s monotonically decreases with the increase of pressure, and it tends to approach a value of 2.0 at positive pressure. The tunable sound velocities have promising applications in nano waveguides and surface acoustic wave sensors.

Acknowledgements The authors would like to acknowledge the generous financial support from the Defense Threat Reduction Agency (DTRA) Grant # BRBAA08-C-2-0130 and # HDTRA1-13-1-0025, the US Nuclear Regulatory Commission Faculty Development Program under contract # NRC-38-08-950, and US Department of Energy (DOE) Nuclear Energy University Program (NEUP) Grant # DE-NE0000325.

References

1. E.F. de Almeida Junior, F. de Brito Mota, C.M.C. de Castilho, A. Kakanakova-Georgieva, G.K. Gueorguiev, Defects in hexagonal-AlN sheets by first-principles calculations. Euro. Phys. J. B **85**(1), 48 (2012)
2. O. Landre, V. Fellmann, P. Jaffrennou, C. Bougerol, H. Renevier, A. Cros, B. Daudin, Molecular beam epitaxy growth and optical properties of AlN nanowires. Appl. Phys. Lett. **96**(6), 061912 (2010)
3. Z.-H. Yuan, S.-Q. Sun, Y.-Q. Duan, D.-J. Wang, Fabrication of densely packed AlN nanowires by a chemical conversion of Al_2O_3 nanowires based on porous anodic alumina film. Nanoscale Res. Lett. **4**(10), 1126–1129 (2009)
4. T. Xie, Y. Lin, G.S. Wu, X.Y. Yuan, Z. Jiang, C.H. Ye, G.W. Meng, L.D. Zhang, AlN serrated nanoribbons synthesized by chloride assisted vapor-solid route. Inorg. Chem. Commun. **7**(4), 545–547 (2004)
5. Q. Peng, W. Ji, S. De, First-principles study of the effects of mechanical strains on the radiation hardness of hexagonal boron nitride monolayers. Nanoscale **5**, 695–703 (2013)
6. H. Sahin, S. Cahangirov, M. Topsakal, E. Bekaroglu, E. Akturk, R.T. Senger, S. Ciraci, Monolayer honeycomb structures of group-IV elements and III-V binary compounds: first-principles calculations. Phys. Rev. B **80**(15), 155453 (2009)
7. Y. Taniyasu, M. Kasu, T. Makimoto, An aluminium nitride light-emitting diode with a wavelength of 210 nanometres. Nature **441**(7091), 325–328 (2006)
8. A. Khan, K. Balakrishnan, T. Katona, Ultraviolet light-emitting diodes based on group three nitrides. Nat. Photonics **2**(2), 77–84 (2008)
9. F. Guinea, M.I. Katsnelson, A.K. Geim, Energy gaps and a zero-field quantum Hall effect in graphene by strain engineering. Nat. Phys. **6**(1), 30–33 (2010)
10. Y. Ma, Y. Dai, W. Wei, C. Niu, L. Yu, B. Huang, First-principles study of the Graphene@MoSe2 heterobilayers. J. Phys. Chem. C **115**(41), 20237–20241 (2011)
11. Z.H. Aitken, R. Huang, Effects of mismatch strain and substrate surface corrugation on morphology of supported monolayer graphene. J. Appl. Phys. **107**(12), 123531 (2010)
12. C. Lee, X. Wei, J.W. Kysar, J. Hone, Measurement of the elastic properties and intrinsic strength of monolayer graphene. Science **321**(5887), 385 (2008)
13. X. Wei, B. Fragneaud, C.A. Marianetti, J.W. Kysar, Nonlinear elastic behavior of graphene: ab initio calculations to continuum description. Phys. Rev. B **80**(20), 205407 (2009)
14. Q. Peng, W. Ji, S. De, Mechanical properties of the hexagonal boron nitride monolayer: ab initio study. Comput. Mater. Sci. **56**, 11 (2012)
15. Q. Peng, W. Ji, S. De, Mechanical properties of graphyne monolayer: a first-principles study. Phys. Chem. Chem. Phys. **14**, 13385–13391 (2012)
16. C.A. Marianetti, H.G. Yevick, Failure mechanisms of graphene under tension. Phys. Rev. Lett. **105**, 245502 (2010)
17. G. Kresse, J. Hafner, Ab initio molecular dynamics for liquid metals. Phys. Rev. B **47**, 558 (1993)
18. G. Kresse, J. Hafner, Ab initio molecular-dynamics simulation of the liquid-metal-amorphous-semiconductor transition in germanium. Phys. Rev. B **49**, 14251 (1994)
19. G. Kresse, J. Furthuller, Efficient iterative schemes for ab initio total-energy calculations using a plane-wave basis set. Phys. Rev. B **54**, 11169 (1996)
20. G. Kresse, J. Furthuller, Efficiency of ab-initio total energy calculations for metals and semiconductors using a plane-wave basis set. Comput. Mater. Sci. **6**, 15 (1996)
21. P. Hohenberg, W. Kohn, Inhomogeneous electron gas. Phys. Rev. **136**(3B), B864 (1964)
22. W. Kohn, L.J. Sham, Self-consistent equations including exchange and correlation effects. Phys. Rev. **140**(4A), A1133 (1965)
23. J. Perdew, K. Burke, M. Ernzerhof, Generalized gradient approximation made simple. Phys. Rev. Lett. **77**, 3865 (1996)
24. P.E. Blöchl, Projector augmented-wave method. Phys. Rev. B **50**(24), 17953–17979 (1994)
25. R.O. Jones, O. Gunnarsson, The density functional formalism, its applications and prospects. Rev. Mod. Phys. **61**(3), 689–746 (1989)
26. Q. Peng, C. Liang, W. Ji, S. De, A theoretical analysis of the effect of the hydrogenation of graphene to graphane on its mechanical properties. Phys. Chem. Chem. Phys. **15**, 2003–2011 (2013)

27. Q. Peng, C. Liang, W. Ji, S. De, A first principles investigation of the mechanical properties of g-tln. Model. Numer. Simul. Mater. Sci. **2**, 76–84 (2012)
28. Q. Peng, C. Liang, W. Ji, S. De, A first principles investigation of the mechanical properties of g-ZnO: the graphene-like hexagonal zinc oxide monolayer. Comput. Mater. Sci. **68**, 320–324 (2013)
29. M. Topsakal, S. Cahangirov, S. Ciraci, The response of mechanical and electronic properties of graphane to the elastic strain. Appl. Phys. Lett. **96**(9), 091912 (2010)
30. J.F. Nye, *Physical Properties of Crystals* (Oxford Science, Oxford, 1995)
31. S.Yu. Davydov, Third order elastic moduli of single layer graphene. Phys. Solid State **53**(3), 665 (2011)
32. Q. Peng, S. De, Tunable band gaps of mono-layer hexagonal BNC heterostructures. Physica E **44**, 1662–1666 (2012)
33. Q. Peng, A.R. Zamiri, W. Ji, S. De, Elastic properties of hybrid graphene/boron nitride monolayer. Acta Mech. **223**, 2591–2596 (2012)
34. F. Everest, *The Master Handbook of Acoustics* (McGraw-Hill, New York, 2001)
35. E.R. Benes, R. Groschl, F. Seifert, A. Pohl, Comparison between BAW and SAW sensor principles. IEEE Trans. Ultrason. Ferroelectr. Freq. Control **45**(5), 1314–1330 (1998)
36. R. Weigel, D.P. Morgan, J.M. Owens, A. Ballato, K.M. Lakin, K. Hashimoto, C.C.W. Ruppel, Microwave acoustic materials, devices, and applications. IEEE Trans. Microw. Theory Tech. **50**(3), 738–749 (2002)